

DEVELOPMENT OF RELIABLE AND MISSION CAPABLE MICRO AIR VEHICLES

Roberto Albertani†, Frank Boria*, Scott Bowman*, Dan Claxton*, Aaron Crespo*, Carlo Francis*, Peter Ifju††, Baron Johnson*, Kyu Ho Lee**, Mike Morton*, Mike Sytsma†
Department of Mechanical and Aerospace Engineering
University of Florida, Gainesville, FL 32611-6250

The University of Florida has a well documented history of developing mission capable Micro Air Vehicles (MAVs). UF has established a successful philosophy that focuses on aircraft reliability and durability. This process incorporates four criteria that apply to both the design of the airframe and selection of components: durability and reliability, minimized form factor, weight reduction, and increased overall efficiency. Despite our best attempts at achieving optimal performance through weight reduction and improved efficiency, often times the durability requirement dominated the design process. This paper documents the design and construction philosophy of the MAVs used for the International Micro Air Vehicle Competition endurance and surveillance missions. The result of this process is well-tested aircraft that meet the design requirements both effectively and consistently through the implementation of a unique flexible wing design.

Nomenclature

AC	= aerodynamic center
AOA	= angle of attack
b_W	= wing span
C_D	= drag coefficient
C_L	= lift coefficient
C_{Lmax}	= maximum lift coefficient
C_M	= pitching moment coefficient about leading edge
C_{VT}	= vertical tail volume coefficient
CG	= center of gravity
L_{VT}	= distance: vertical tail AC to wing AC
MAC	= mean aerodynamic chord
S_{VT}	= vertical tail surface area
S_W	= wing surface area
SM	= static margin
Re	= Reynolds number
RPM	= revolutions per minute
V	= free stream velocity
x_{AC}	= location of aerodynamic center on wing
x_{CG}	= location of center of gravity on wing

I. Introduction

IN recent years, Micro Air Vehicle (MAV) development at the University of Florida (UF) has garnered much interest in real-world applications.

The MAV Laboratory at UF specializes in the design and creation of small mission capable aircraft under multiple contracts. In addition to contractual work, the UF MAV team has competed in the International MAV Competition (IMAVC) the past 8 years and has won first place 6 consecutive years.

The team attributes much of its success to the thin, flexible wing design developed at UF^{1,2}. Studies have shown that thin wings have a distinct advantage over volumetric wings at the low Reynolds numbers where MAVs typically operate³⁻⁵. The batten reinforced wing design (BR-wing) utilized in the 2004 UF MAV was improved upon with a perimeter reinforced wing (PR-wing) design, shown in Fig. 1. The PR wing was wind tunnel tested and exhibited increased lifting abilities at flight speeds. The 2005 UF MAV will utilize the PR-wing in the IMAVC. The BR and PR carbon fiber reinforced elastic membrane wings are illustrated in Fig. 2.



Figure 1. Picture of aircraft with perimeter reinforced (PR) wing

† Graduate Student

†† Professor

* Undergraduate Student

** Research Assistant

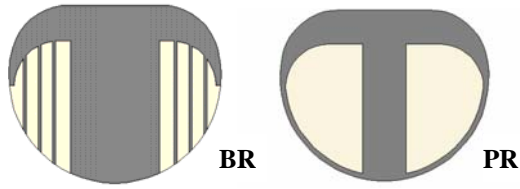


Figure 2. Planform of BR-wing vs. PR-wing

The 2005 IMAVC consists of a series of missions, each with unique challenges associated with its objective. This paper will focus on the surveillance and endurance missions. The surveillance mission requires a MAV to fly 600 m from the launch site and acquire a clear image of a 1.5 m x 1.5 m alphanumeric target. The endurance mission requires a MAV to remain airborne for as long as possible, with a 900 second maximum recorded time. The scores of both missions are heavily weighted towards the minimization of aircraft maximum dimension.

In order to be successful at the 2005 IMAVC, the UF MAV Team developed MAVs capable of reliably completing these mission objectives in a wide range of weather conditions. Selection of reliable and durable electronic components was a focus point for the 2005 UF MAV design, and aircraft were constructed utilizing modern composite fabrication methods. The PR-wing was evaluated with wind tunnel tests and compared against the BR-wing. Aircraft utilizing both wing types were flight tested to ensure mission capability while also minimizing the maximum dimension in order to maximize score.

II. Design Procedure

This section will detail the design procedure that UF has established for the development and creation of mission-capable MAVs. Component selection, wing and fuselage design, vertical stabilizer sizing, and stability requirements will be discussed.

A. Component Selection

The design process was started by considering previous winning aircraft as a baseline. Factors which contributed to the success of the previous years' aircraft were determined through careful consideration. Overall, it appeared that the airframe designs were very much dependent upon the size, shape, and weight of the electronic components. However, it was found that the most successful aircraft utilized the more durable and reliable components as opposed to aircraft with less reliable components.

The UF MAV team began to design its endurance and surveillance entries into the 2005 IMAVC with several criteria to guide the design process. In the past, the UF MAV team has encountered difficulty in the reliable use of extremely

lightweight off-the-shelf electronic components. Most of the electronic components tested did not match their listed specifications, and many of the components experienced reliability and durability problems. The criteria regarding the selection of components were ranked in order of importance as follows:

1. Durability/reliability
2. Overall size/form factor
3. Weight
4. Power efficiency

A list of suitable components was compiled for each mission. The individual components were both bench tested and employed in flying aircraft. The performance of individual components were compared against each other and selected based on suitability for each mission (Table 1 and Table 2).

Feigao released several brushless electric motors which exhibited higher average power outputs than the Maxon RE-10, the motor used in the 2004 UF MAV¹. The Feigao motors have proven beneficial because they did not have delicate brushes and used larger diameter shafts than the RE-10, making them much more durable. The Feigao motor weighed 0.9 g more than the RE-10, but the higher average power output made it the better choice for the surveillance mission. The current draw of the Feigao motor was too high for an endurance craft but was inconsequential for the short flights of the surveillance craft (Table 1).

Table 1. Component breakdown for surveillance aircraft

	Component	Qty.	Wt. (g)	I _{max} (mA)
Motor	Feigao (128430S)	1	10.8	2500†
ESC	YGE4-BL	1	2.4	30
Receiver	GWS R-4P	1	4.0	30
Servo	Cirrus CS-4.4	2	3.4	150
Battery 1	ETEC 210 mAh	2	4.9	N/A
Battery 2	Didel 30 mAh	2	0.9	N/A
Camera	Micro B/W CMOS	1	0.9	2
Video TX	RF-Links SDX-22	1	2.0	68
Total		11	38.5	2780

Testing showed that the smallest and lightest servos exhibited poor centering and resolution. Additionally, these servos were very fragile and would often be damaged on landing. These problems led to the selection of the Cirrus CS-4.4 and Bluebird BMS-303 servos. These two servos demonstrated adequate resolution, centering, and durability. The gearing and construction of the two servos were

† Tests performed using GWS 3030 65 mm propeller

similar, but it was found that the Bluebird servo consumed less current than the CS-4.4. The lower current consumption of the Bluebird servo made it the more desirable servo to use on both aircraft, but due to the low availability of Bluebird servos they were chosen for use in the endurance aircraft while the surveillance craft utilized the more readily available CS-4.4.

Table 2. Component breakdown for endurance aircraft

	Component	Qty.	Wt. (g)	I _{max} (mA)
Motor	Maxon (118392)	1	9.8	700†
Receiver	Penta	1	2.3	25
Servo	Bluebird 303	2	3.2	80
ESC	Pixie – 7P	1	1.5	20
Battery	Etech 250 mAh	2	5.6	N/A
Total		7	31.2	825

Batteries were tested and compared against each other utilizing the West Mountain Computerized Battery Analyzer. Four types of battery packs were discharged at 0.7 A and voltage vs. time plots were obtained (Fig. 3). It was determined from these tests that the ETEC 250 mAh battery would be the most suitable choice due to its extended discharge time and higher discharge capability.

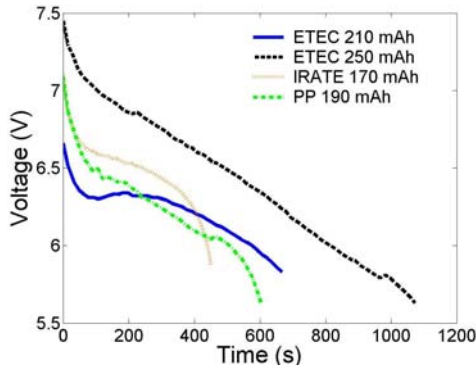


Figure 3. Two cell battery discharge time history for a discharge rate of 0.7 A

In previous years it was noted that the surveillance video transmission was adversely affected by interference and often suffered from video cutouts. It was determined that the video cutouts were caused when the motor temporarily drew excessive current and the battery voltage dropped below the operating requirements of the video system. The feedback from the electronic speed control (ESC) and motor were found to be the main

causes of the interference. In an attempt to eliminate these problems the video system was powered by a separate battery. Tests showed that the Didel 30 mAh battery would provide enough power to the video system to maintain transmission for 23 minutes. The separate battery system proved successful in reducing video cutouts and interference.

B. Airframe Geometry

The design of the airframe began with a target maximum dimension. The target maximum dimension was chosen based off of historical trends and was scaled down from the 2004 UF MAV design. This year appropriate selections of maximum dimension were realistically set at 12.7 cm for surveillance and 10.8 cm for endurance.

After a maximum airframe dimension was chosen, the design of the aircraft was rendered using computer aided design (CAD) software. The airfoil selected was the one used on the 2004 UF MAV¹. The wing design follows naturally from the maximum dimension; the wing should have as much area as possible and still provide space for the protrusion of the motor and propeller, while staying within the size envelope. Additionally, a reference CG position was established based off of flight tests and historical data. A spreadsheet was employed which used component weights and placements to find where the most likely CG position would be and compared that value against the reference. If there was significant discrepancy, the wing was redrawn to better match the calculated and historical CG positions.

In order to design a fuselage the components were drawn to scale in an aircraft configuration and a fuselage with the smallest form factor was lofted around them. The top of the fuselage was designed such that it would mate seamlessly with the wing.

The vertical stabilizers were then sized⁶. It was determined that for the UF MAV it was most appropriate to define separate vertical tail volume coefficients for the surfaces above and below the wing. The vertical tail volume coefficient is defined as:

$$C_{VT} = \frac{L_{VT} S_{VT}}{b_w S_w} \quad (1)$$

The C_{VT} of the 2004 UF MAV was calculated to be 0.0446 for the bottom stabilizer and 0.0363 for the top stabilizer; hence the overall vertical tail volume coefficient was 0.0810. In an attempt to increase stability during launching the stabilizer above the wing was replaced with two stabilizers offset from the centerline of the aircraft. The stabilizers required resizing in order to fit within the maximum dimension envelope, and the resulting C_{VT} of the top

† Tests performed using U-80 propeller trimmed to 64 mm

stabilizer resulted in 0.0546, a 22.5% increase in the overall vertical tail volume coefficient.

Once the wing and fuselage sketches were completed they were further analyzed and prepared for production. A wing with complex curvatures like the UF MAV was cumbersome to create using existing CAD technology, thus a new tool was implemented to alleviate this frustration. MAVLab (Fig. 4), a Matlab®-based program written by the UF MAV team, was utilized to design the complex 3D shape of the wing. MAVLab contains tools to design and modify wing geometry rapidly as well as calculate the surface area, aerodynamic center (AC), and mean aerodynamic chord (MAC) for later analysis. One important parameter that was derived from this data is the static margin (SM), defined as:

$$SM = \frac{x_{AC} - x_{CG}}{MAC} = -\frac{dC_M}{dC_L} \quad (2)$$

The CG of the aircraft can therefore be determined given a known AC and a desired static margin. For the case of the UF MAV, experience has shown that a static margin of 10-15% was necessary for comfortable pilot controlled flight.

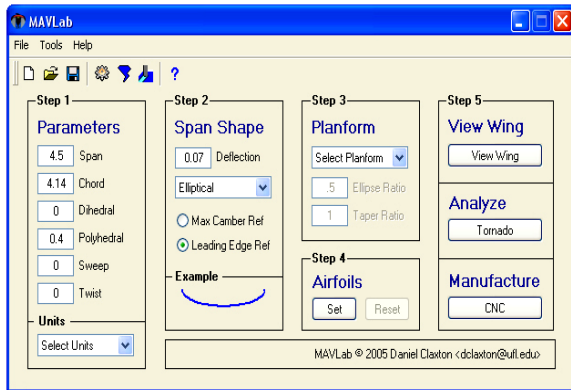


Figure 4. MAVLab graphical user interface. MAVLab has the capability to modify wing span, chord, dihedral, polyhedral, sweep, twist, airfoil shape, and airfoil distribution

After the wing was modeled within MAVLab as shown in Fig. 5, it was exported to Tornado⁷, a freely distributed inviscid vortex lattice solver. Tornado© was used to calculate all the forces and moments applied to the wing by a given inviscid flight condition. The force output from Tornado© did not compare favorably to wind tunnel data and could not be directly used to determine actual forces on the aircraft. However, Tornado© was tremendously useful for the purpose of determining trends in the pitching moment, which compared well to wind tunnel data.

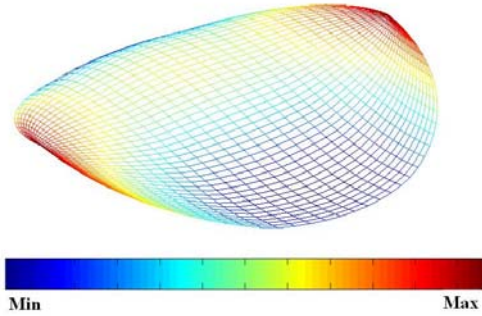


Figure 5. MAVLab wing visualization with intensity representing out of plane displacement

Tornado© was used to determine how pitching moment changed with respect to lift for any given wing design. This information was used to determine the stability derivative dC_M/dC_L which was used to verify the SM in (2).

III. Construction

This section details the construction methods developed by the UF MAV team for its 2005 entries into the IMAVC. A computer numerically controlled (CNC) milling machine was utilized to create tools for composite lay up. Carbon and aramid composites were used to create airframe components and these were then assembled.

A. Airframe Tool Creation

MAVLab has the capability to export tool path files, which are sets of instructions for a CNC milling machine. The advantage of this feature was the ability to mill wing tools that were exact representations of the CAD designs created in MAVLab (Fig. 6). This ensures perfect symmetry and consistent geometry, which is critical to the reliable performance of mission capable MAVs.

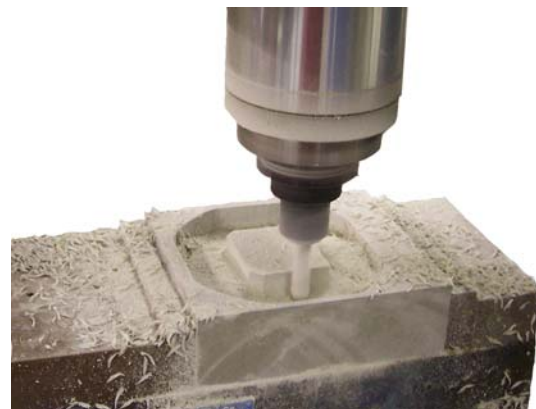


Figure 6. Wing tool milled on CNC milling machine

The tools were made of high density, high temperature tooling board which offered three desirable characteristics.

- Heat resistance
- Fast milling
- Ease of surface finish

The heat resistance was paramount because the tool must endure the heat of a cure cycle for every part produced. Milling allowed for rapid, reproducible prototyping and reduced labor. After milling, the surface of a wing tool was not perfectly smooth. The ridges that remained were lightly sanded with fine grit sand paper. Although the tooling board was dense, it sanded easily in a very short amount of time to a smooth finish.

In order to craft reproducible wings, lay up patterns were required to show where the unidirectional carbon strips should be placed. Past designs used patterns printed onto paper and then adhered to the tool underneath the release film. This process proved problematic for more complex curved wings because the 2-dimensional paper did not conform well to the tool. To avoid this problem, MAVLab was modified to create CNC tool paths that could trace custom patterns onto the 3-dimensional wing surface with a permanent marker. A completed wing tool is shown in Fig. 7.



Figure 7. Completed wing tool ready for composite lay up process

B. Composite Construction

UF's MAV construction has consistently implemented composites in airframe structure. The advantages of composites in aerodynamic structures were three-fold:

- High strength
- Low weight
- Easy formability over complex surfaces

The primary composite utilized was carbon fiber and thermo-set epoxy in a pre-impregnated form which demonstrated very high strength and flexibility after cure. The carbon fiber cloth used in construction was a 0/90° plain weave, 176.3 g/m², 3000 fiber/yarn

pre-impregnated fabric. In addition, pre-impregnated unidirectional carbon fiber was used. Despite the high strength of the carbon fiber, 17 g/m² aramid cloth reinforcement was required to prevent crack propagation in the 0/90° weave cloth on the wing leading edge.

Extreme care was taken in the wing lay up procedure to take advantage of the precision allowed by the CNC wing tools. No viable automated process was available to lay up the wings, so the UF MAV team developed a procedure for composite construction of the airframe. The following steps document the process.

1. Wing construction required the application of Teflon release film to the wing tool using Elmer's spray glue.
2. The leading 20% of the wing was constructed of a single layer of 0/90° cloth oriented at a 45 degree angle with respect to the chord line. The 0/90° cloth was then reinforced by a single layer of aramid cloth.
3. One mm strips of unidirectional carbon fiber were cut from a sheet of pre-impregnated material using a custom built carbon strip-cutting tool
4. The portion of the wing that attached to the fuselage was made by meticulously applying layers of the unidirectional carbon fiber strips to a pattern drawn on the tool (Fig. 8). The unidirectional carbon fiber was layered for strength and rigidity and was interwoven at intersections to create stronger mechanical joints. The primary structure of the wings was identical for the PR and BR wings, but the areas to be covered by latex were different. The PR-wing was constructed by adding two layers of unidirectional carbon fiber along the trailing edge.

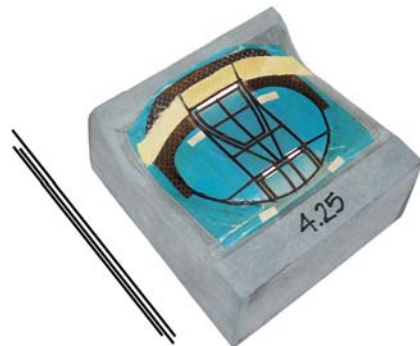


Figure 8. Steps 1, 2, and 3 of composite construction completed

The BR-wing was constructed by adding 3 battens parallel to the chord line consisting of 2 layers of unidirectional carbon fiber each. A single layer of vacuum-bag material was applied in the center section of the wing which provided a durable, light-weight surface for the hatch and elevator and doubled as hinge material for both.

5. Teflon release film was applied to the fuselage tool. The complex curvature of the fuselage tool required separate layers of 0/90° cloth to be applied to each side of the tool, and the layers were overlapped over the centerline. The fuselage was then placed on a plate which was shaped to the curvature of the wing (Fig. 9).
6. The wing and fuselage were covered with porous Teflon release film and placed in a vacuum bag. The bag was sealed and a vacuum was drawn to a pressure of 0.01 atm absolute and placed in an oven at 130° C for 4 hours.



Figure 9. Fuselage laid up on tool

C. Assembly

7. Once removed from the cure cycle, the composite wing and fuselage were trimmed and joined using cyanoacrylate (CA) adhesive (Fig. 10).



Figure 10. Wing and fuselage joined with CA

8. Connectors were soldered to the receiver and ESC.
9. Electric motor, ESC, receiver, and servos were installed inside the fuselage. The servos were mounted by adhering them to the carbon fiber wall with two-sided tape and lashing them with aramid thread (Fig. 11). The motor was installed with a 5° declined thrust line with respect to the wing.



Figure 11. Servos installed in fuselage with motor and radio

10. The wing was skinned with 0.25 mm latex rubber. The latex was applied by masking then coating all contact surfaces of the wing with Elmers spray glue. Then the latex was permanently adhered with CA glue and trimmed.
11. Two vertical stabilizers were adhered to the top of the wing using CA glue.

IV. MAV Wind Tunnel Performance

A. Wind Tunnel Load Data

The performance of the UF MAV was extensively studied in UF's Low Speed, Low Turbulence (LSLT), open circuit, 0.9 m x 0.9 m x 2.0 m test section wind tunnel. The wind tunnel was capable of a maximum test section velocity of 15 m/s and was equipped with a calibrated 6 component sting balance connected to a computer data sampling system. The wind tunnel was calibrated to exhibit turbulence levels of less than 0.5% at 10 m/s. The sting balance was connected to a computer controlled servo arm that could accurately change angle of attack (AOA). The tunnel was controlled by a suite of programs that gathered data over an AOA sweep at a given airspeed⁸.

UF has been continuously researching many variations of the MAV wing and has produced the

PR-wing, a new flexible wing structural design which has substantially different flight qualities than the 3 batten wing used on the 2004 UF MAV¹.

Lift, drag, and pitching moment data were gathered at velocities ranging from 6 m/s to 13 m/s using 15.24 cm span BR and PR-wings attached to identical fuselages. The propeller was excluded from the tests which allowed for airframe aerodynamic characterization only. It was very likely that the inclusion of a powered propeller would have an effect on airframe aerodynamics, and wind tunnel tests are planned which will include a powered propeller on a MAV.

Initial wind tunnel tests indicated an increase in the maximum lift coefficient and critical AOA at speeds below and including 10m/s as shown in Fig. 12. The increase in C_{Lmax} showed potential to allow for decreased flight speeds or smaller aircraft^{9,10}.

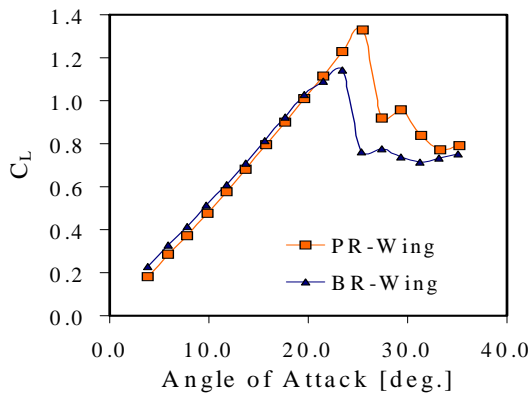


Figure 12. Lift coefficient vs. angle of attack

Further data analyses showed that the C_L/C_D ratio, a general measure of wing efficiency, was higher for the PR-wing than it was for the BR-wing for all flight lift coefficients (Fig. 13). Considering the PR-wing had a higher C_L/C_D for most flight conditions, it could be deduced that the throttle could be set lower in flight and hence endurance could be increased.

The increase of C_{Lmax} in the PR-wing was further shown in a C_D^2/C_L^3 plot prepared for both models. Minimizing the C_D^2/C_L^3 metric over the range of C_L will yield the most efficient cruise condition for an aircraft if such a flight condition is possible. Figure 14 shows that each C_D^2/C_L^3 plot is essentially constant after a C_L of 0.6. The curve for the PR-wing extends to a higher C_L than the BR-wing which indicates that the PR-wing will fly within a larger highly efficient range, simplifying pilot control.

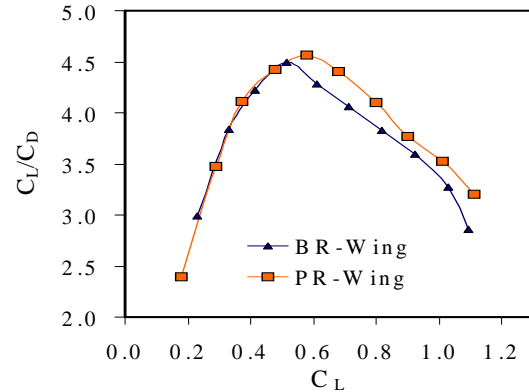


Figure 13. Lift over drag coefficients vs. lift coefficient for $V = 10$ m/s, $Re = 99,500$

Calculations were performed which compared the power required for flight and the power available from the Maxon RE-10 motor and a modified U-80 64mm propeller. A thrust calibration curve was determined in order to calculate a power available plot. A wing loading curve was found to determine a power required plot. This data was used to create Fig. 15. A reasonable maximum RPM value of 17,500 was chosen to represent maximum available power, and the actual weight and size of the endurance aircraft was utilized. A power available curve was also added to illustrate the minimum RPM required for marginal flight.

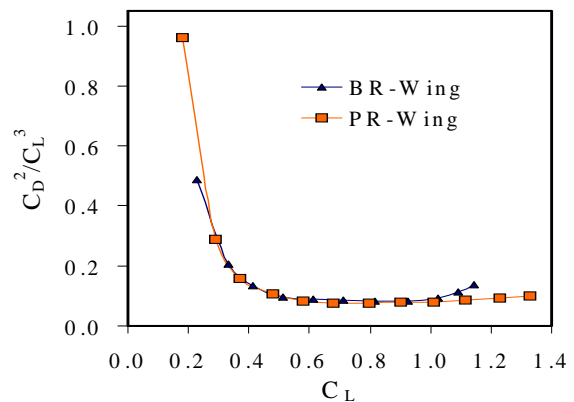


Figure 14. C_D^2/C_L^3 vs. lift coefficient for $V = 10$ m/s, $Re = 99,500$

The point where the power required and power available curves intersect indicates the maximum airspeed possible. The difference between the power available and power required curves is a useful metric to determine climb out capabilities.

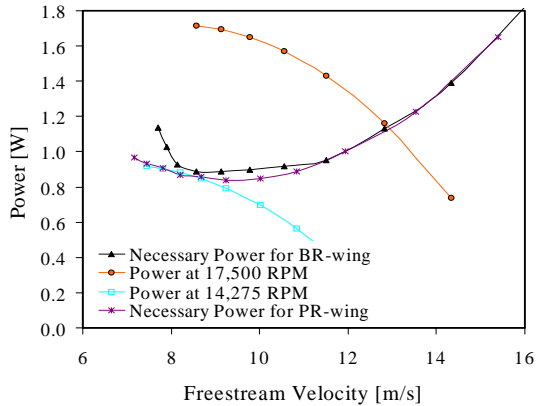


Figure 15. Power required, maximum power available, and marginal power available for 4.25", 38 g BR-wing aircraft

Wind tunnel analysis also gave rise to valuable data regarding pitch stability. Tests indicated that the magnitude of the slope of C_M vs. C_L curve was greater with the PR-wing than the BR-wing, hence the SM of the PR-wing is greater than the SM of the BR-wing (Fig. 16). This data indicated that the AC of the PR-wing is aft of the AC for the BR-wing for normal flight conditions.

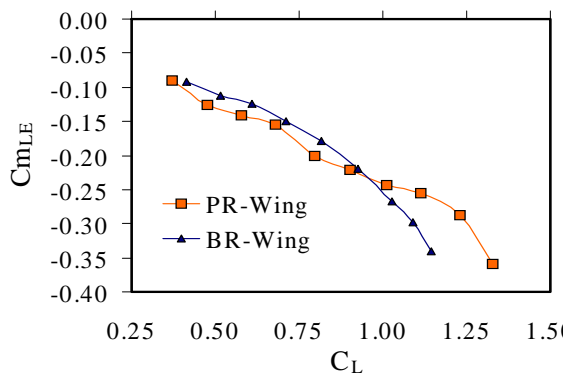


Figure 16. Pitching moment coefficient vs. lift coefficient for $V = 10$ m/s, $Re = 99,500$

B. Wind Tunnel Visualization Data

In order to better understand the flow properties of the PR-wing, models were studied using the Particle Image Velocimetry (PIV) flow visualization technique in the wind tunnel. The PIV system used two Nd:YAG 50 mJ lasers directed through a barrel lens to form a laser sheet. The laser sheet was aligned parallel to the flow and the wing surface normal. A smoke generator attached to a seeder tube injected seed particles into the inlet of the wind tunnel. A high speed digital camera gathered images of the illuminated seed particles flowing around the wing. The laser was aligned over the same location on the

BR-wing and the PR-wing models and tested at a speed of 10 m/s.

The PR-wing demonstrated a large flow separation bubble at the leading edge which first formed at an AOA of 6° . The separation bubble was observed to re-attach at the point where the latex membrane joins the carbon leading edge, and the wake of the bubble shed uniformly sized turbulence. The BR-wing did not show any leading edge separation until an AOA of 18° . It also displayed a laminar to turbulent transition around the one third chord location for most angles of attack, but the turbulence was much more disordered than the wake of the separation bubble. The PR-wing trailing edge boundary layer (BL) was more constant than that of the BR-wing indicating strong trailing edge flow attachment due to turbulence. This attachment supports the higher C_{Lmax} value, and it was seen that at very high angles of attack the BR-wing flow separated completely while the PR-wing maintains some attached flow. Images of the leading edges of the PR-wing and BR-wing are shown in Figs. 17, 18.

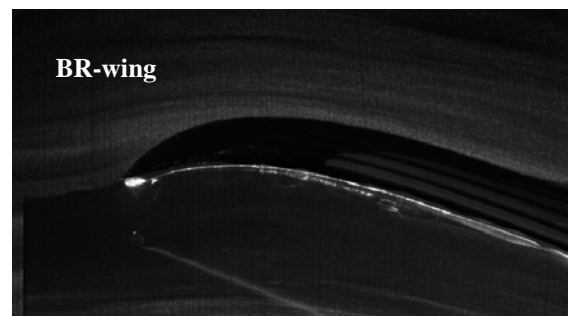


Figure 17. Leading edge flow visualization image for BR-wing

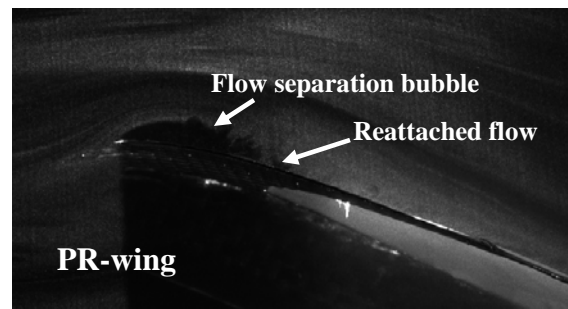


Figure 18. Leading edge flow visualization image for PR-wing, angle of attack 15°

The PIV system was utilized to output pressure coefficient data. This indicated very high flow velocities concentrated around the leading edge separation bubble of the PR-wing. The BR-wing exhibited a more distributed velocity profile over the top surface of the wing. The pressure coefficient contour plots of both wings are shown in Figs. 19 and 20 with blue denoting low pressures and red denoting

high pressures. It can be deduced from this information that the separation bubble affects the pressure distribution around the wing. The pressure distribution directly affects the AC of the wing and therefore the SM of an aircraft.

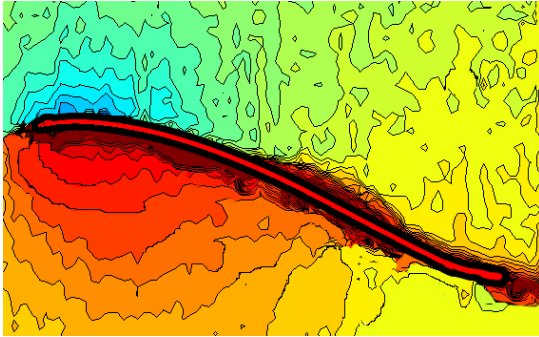


Figure 19. Pressure coefficient contour plot for BR-wing

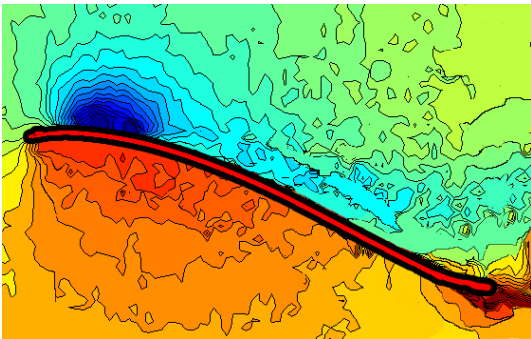


Figure 20 Pressure coefficient contour plot for PR-wing

C. Wind Tunnel Wing Displacement Data

The wind tunnel has recently been instrumented with unique equipment for measuring the 3-D deformations of wings under wind load. Visual Image Correlation (VIC) hardware including stereo digital cameras and software purchased from Correlated Solutions Inc. was used for high resolution measurements of displacement and strain on the PR and BR wings. The results shown in Fig. 21 illustrate pronounced billowing of the PR wing under load. It was shown that the deformation magnitude was a function of wind speed and angle of attack¹².

It is speculated that the geometric discontinuity where the latex meets the carbon fiber and initiates billowing causes a steady state recirculation. It is unclear however why reattachment is so dependable and warrants further study.

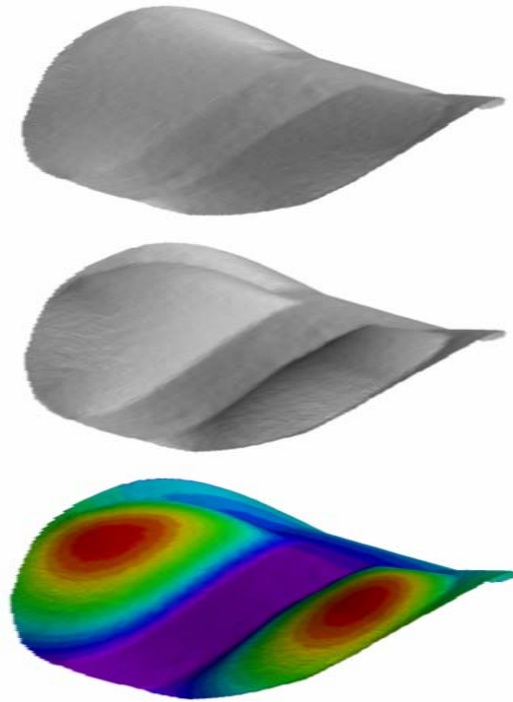


Figure 21. VIC displacement data for $V = 0$ (top) and $V = 13$ m/s (middle & bottom), $AOA = 12^\circ$

V. Flight Testing

Flight testing was a crucial phase in the development of the UF MAV. It provided an opportunity to qualitatively verify the data obtained from wind tunnel tests, as well as assess and refine handling and stability characteristics. In addition, mission capability was thoroughly tested through flight testing in a wide range of weather conditions.

A flight testing procedure was established for the assessment of MAVs at UF. For initial tests, control surface deflections and the CG position were set based on prior experience. After hand launching, any pitch or roll tendency was corrected with control surface trim until tracking was acceptable. Often, MAVs endured a number of impacts during the trimming procedure, so the reliability and durability of the airframe and all components was assessed and any failure modes identified.

Once an adequate trim condition was established, maneuverability and controllability was examined. Both left and right turns of various radii as well as climbs and descents were performed. Qualitative feedback from the pilot led to iterative changes in the control surface actuation as well as CG position.

Control surface actuation was modified to allow for a gentle feel around neutral in order to prevent over control. The CG position was iteratively varied

until a position was found which offered a high degree of longitudinal and directional stability, yet provided appropriate maneuverability for the mission objective. It has been previously found that under gusty wind conditions, the CG position must be moved forward in order to maintain a reasonable pilot workload¹¹.

Flight tests were performed on MAVs with PR, BR, and nominally rigid wings. Pilot feedback consistently favored the BR and PR-wings over the rigid wings. The most significant characteristics from a piloting standpoint were smoother control response and slower flight speeds. Also, in gusty wind conditions the PR and BR-wings required significantly lower pilot workload as compared to the rigid wings.

Flight testing of the PR-wing verified the wind tunnel data which suggested the center of pressure would be located farther aft than on other wing designs. Originally, the PR-wing aircraft required significant up-elevator trim and exhibited inadequate elevator effectiveness, which led to shifting the CG aft. With the proper CG position, an appropriate balance between longitudinal stability and maneuverability was established.

The PR-wing also exhibited stable, maneuverable flight at higher angles of attack and slower flight speeds than other wing designs. This characteristic correlated with wind tunnel data, which stated that the PR-wing provided a higher critical AOA and a greater maximum coefficient of lift. In qualitative flight testing analysis, this translated into greater pull-out capability and tighter turn radii as well as a larger airspeed operating envelope. As a result, the PR-wing completed the surveillance mission objective in winds as strong as 30 km/hr. Additionally, the PR-wing completed the endurance mission by sustaining controllable flight for 16 minutes.

VI. Conclusion

The success found in analysis and flight testing of the UF MAV validated the long-standing design philosophy established by UF, which was founded on experience and emphasized reliability and durability. The unique design iteration process and construction methods developed by UF have resulted in MAVs capable of reliable completion of their mission objectives.

Loads testing, PIV, and VIC provided insight into the behavior of the PR-wing under various flight conditions. Loads testing clearly indicated the PR-wing provided a higher C_{Lmax} and critical AOA than the BR-wing. PIV analysis supported loads testing data by showing the turbulence shed by the separation bubble, which helped to maintain flow

attachment on the PR-wing. VIC produced high resolution deformation of the flexible membrane wing under flight loads and will help to provide future insight into the physics of flexible wings.

Observations made in flight testing verified the capability of the PR-wing to maintain a higher AOA and slower flight speeds than other wing designs. Flight tests also verified the durability of the airframe subjected to repeated impact trauma. These characteristics attributed to mission capability, which was demonstrated through successful simulated missions during flight testing.

References

- ¹Albertani et. al., "University of Florida Biologically Inspired Micro Air Vehicles," 2004 IMAVC Competition.
- ²Ifju, P., Jenkins, D.A., Ettinger, S., Lian, Y., Shyy, W., & Waszak, M.R., "Flexible-Wing-Based Micro Air Vehicles," AIAA Annual Conference, AIAA 2002-0705, Jan. 2002.
- ³Albertani, R., Hubner, J.P., Ifju, P., Lind, R., and Jackowski, J., "Experimental Aerodynamics of Micro Air Vehicles," *SAE World Aviation Congress and Exhibition*, Paper 04AER-8, Nov 2004.
- ⁴Lian, Y., Shyy, W., Ifju, P., "Membrane Wing Model for Micro Air Vehicles," *AIAA Journal*, Vol. 41, No. 12, pp.2492-2494, Dec. 2003.
- ⁵Ifju, P., Jenkins D.A., Ettinger S., Lian Y. and Shyy W., "Flexible-Wing-Based Micro Air Vehicles", AIAA 2002-0705.
- ⁶Yechout, T., *Introduction to Aircraft Flight Mechanics: Performance, Static Stability, Dynamic Stability, and Classical Feedback Control*, AIAA, 2003.
- ⁷Merlin, T., Tornado, Software Package, Ver. 1.28b, <http://www.ave.kth.se/divisions/aero/software/tornado/>, Nov 2004.
- ⁸Albertani, R., Hubner, P., Ifju, P., Lind, R., "Wind Tunnel Testing of Micro Air Vehicles at Low Reynolds Numbers," SAE World Conference, Reno, NV, November 2004.
- ⁹Hoerner, Sighard F. and Borst, Henry V., *Fluid-Dynamic Lift: Information on Lift and its Derivatives, in Air and in Water*, published by Liselotte Hoerner, 1992.
- ¹⁰Hoerner, Sighard F., *Fluid-Dynamic Drag: Information on Aerodynamic Drag and Hydrodynamic Resistance*, published by Liselotte Hoerner, 1995.
- ¹¹Jenkins, D.A., Ifju, P., Abdulrahim, M., & Olipra, S., "Assessment of the Controllability of Micro Air Vehicles," Micro Air Vehicle Conference, Bristol England, April 2001.
- ¹²Albertani, R., Stanford, B., Hubner, J. P., Lind, R. and Ifju, P., "Experimental analysis of deformation for flexible-wing Micro Air Vehicles," *AIAA SDM Conference*, Paper, Austin, TX, 2005.